

Cirrus cloud microphysics and its dependency on aerosol type, temperature, and cooling rate

AIMS AND SCOPE:

Cirrus clouds are of great importance for the global radiative balance. The order of magnitude of an anthropogenically caused radiative forcing of these clouds remains highly uncertain (IPCC, 1999). For a more accurate evaluation of this impact, a better understanding of the microphysical processes leading to cirrus formation and their resulting optical properties is crucial. Up to now there have only been few field studies examining the factors controlling the ice nucleation processes and the optical properties of cirrus clouds (e.g. INCA, Ovarlez et al., 2002; CRYSTAL-FACE, Jensen et al., 2004).

We present results of detailed laboratory measurements of homogeneous and heterogeneous ice nucleation, performed at the aerosol chamber AIDA under simulated atmospheric cirrus conditions. The experiments were conducted at temperatures between 238 and 185 K and cooling rates between -0.3 and -3.0 K min^{-1} . Fully dissolved sulphuric acid and ammonium sulphate droplets were used during homogeneous ice nucleation experiments, while pure soot, soot coated with sulphuric acid or ammonium sulphate as well as two types of mineral dust served as nuclei for heterogeneous ice formation. We focus on the influence of aerosol type, temperature, and cooling rate on the ice crystal number concentration of the formed ice clouds. The freezing threshold relative humidities over ice for the different aerosol types are also addressed.

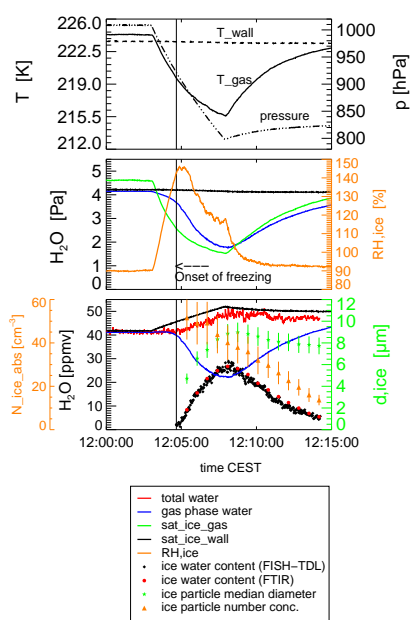
EXPERIMENTALS:

The AIDA aerosol chamber is a large evacuable vessel which can be cooled down to 183 K. The pressure range is from 0.1 hPa to 1000 hPa. At constant wall and gas temperature, ice saturation is maintained by a thin ice layer on the chamber walls. The ice supersaturation necessary for homogeneous or heterogeneous formation of ice crystals is achieved by volume expansion due to controlled pumping. The onset of ice formation is precisely detected by measuring the increasing intensity and depolarisation of laser light back-scattered by the growing ice particles. The Lyman- α fluorescence hygrometer FISH (Zöger et al., 1999) measures the total water (gas phase + condensed phase). Simultaneously, the gas phase water concentration is directly measured in-situ by absorption at 1370 nm with a tuneable diode laser (TDL). The total aerosol number concentration is measured with a CNC3010 (TSI). For details of the instrumentation and of the ice nucleation experiments see Möhler et al., 2003.

Ice particle number concentration and size is retrieved both from FTIR extinction spectra and from two optical particle spectrometers (PCS2000 and WELAS, Palas). A detailed description of the FTIR measurements and the error estimation for the ice crystal parameters can be found in Mangold et al., 2004).

The soot particles are produced by a Graphite sparc generator. The two types of mineral dust are Arizona Test Dust (Powder Technology Inc., USA) and Saharan surface dust, respectively. The mean diameters of the aerosol particles used during our experiments were between 0.1 and 0.5 μm .

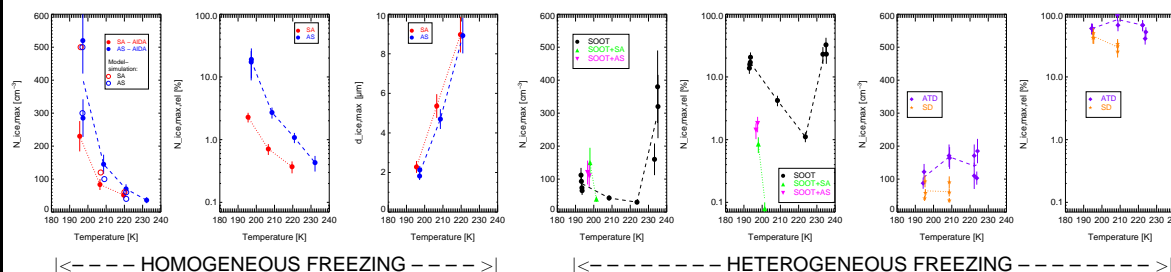
Typical Ice Nucleation Experiment



The figure illustrates – as an example – an ice nucleation experiment in the AIDA chamber with sulphuric acid aerosol at 224 K. The upper panel displays the total pressure as well as the gas and wall temperature inside the chamber. The middle panel displays the water vapour pressure of the gas phase, the ice saturation pressure with respect to gas and wall temperature, and the relative ice saturation with respect to wall temperature, the ice water content retrieved from FISH-TDL data and from FTIR spectra, and the ice crystal concentration and median diameter. The partial pressure of water vapour e_{gas} is controlled by the saturation vapour pressure over ice of the slightly colder ice coated walls $e_{\text{sat,ice,wall}}$. With the start of pumping, e_{gas} decreases almost linearly with the decreasing total pressure. Due to the expansion cooling, the ice saturation pressure $e_{\text{sat,ice,gas}}$ exponentially decreases with decreasing gas temperature and therefore the relative humidity with respect to ice RH_{ice} increases. As soon as RH_{ice} exceeds the critical ice saturation $\text{RH}_{\text{ice,max}}$, ice particles begin to form.

The difference between $e_{\text{sat,ice,wall}}$ and e_{gas} causes a continuous flux of water vapour from the wall into the gas phase. After ice particles have formed, they start to take up the excess water and grow as long as $\text{RH}_{\text{ice}} \geq 100\%$. This additionally lowers e_{gas} and therefore increases the water vapour flux from the wall, resulting in a marked increase of the total water signal. When pumping is stopped, the gas temperature starts to increase, RH_{ice} drops below 100% and the ice crystals start to evaporate. The gas phase water increases due to the evaporating ice crystals and the still existing gradient from $e_{\text{sat,ice,wall}}$ to e_{gas} .

Ice crystal number and size – dependency on aerosol type and temperature

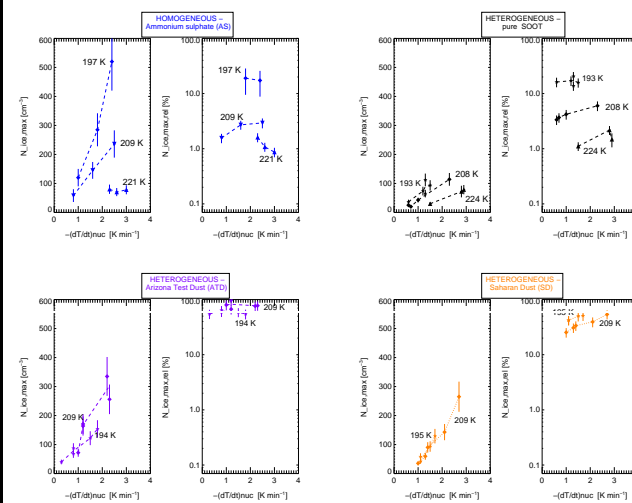


The figures show the maximum ice crystal number concentration both in absolute numbers ($N_{\text{ice,max}}$, cm^{-3}) and as fraction of particles acting as ice nuclei ($N_{\text{ice,max,rel}}$, in percent of the total initial aerosol number concentration N_{aero}) depending on temperature and for the different types of aerosols. For sulphuric acid (SA) and ammonium sulphate (AS) aerosol (left three panels) also the maximum median diameter of the ice crystals is shown. The fourth and fifth panel show the results for pure soot (SOOT), soot coated with sulphuric acid (SOOT+SA) and soot coated with ammonium sulphate (SOOT+AS). The right two panels show the results for Arizona Test Dust (ATD) and for Saharan dust (SD).

The cooling rates at ice nucleation were between -1.3 and -2.0 K min^{-1} . It is important to know that N_{aero} was different for each experiment ($500 - 50000$ cm^{-3}). The error bars reflect the uncertainties of the particle measurements (not standard deviations). The median diameters for all other ice nucleation freezing experiments show nearly the same behaviour like in the third panel. This means that for the dynamical growth of the ice crystals the thermodynamic conditions for water transport and uptake are crucial rather than the aerosol type.

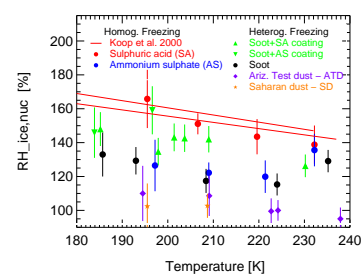
Using the freezing nucleation rates of Koop et al. (2000), Kärcher and Lohmann (2002a,b) developed a microphysical parameterization of homogeneous freezing of supercooled solution droplets, showing that the ice crystal number density in cirrus clouds can mainly be described as a function of updraft velocity (i.e. the cooling rate) and temperature. They also stated that the relationship between total aerosol and ice crystal number in homogeneously formed cirrus clouds is much weaker than in liquid water clouds (i.e. total aerosol number and cloud condensation nuclei). It can be seen that there is good agreement between our measurements and the parameterization (leftmost panel). As N_{aero} was highly variable in our experiments this confirms the weak influence of N_{aero} on $N_{\text{ice,max}}$.

Ice crystal number – dependency on aerosol type and cooling rate



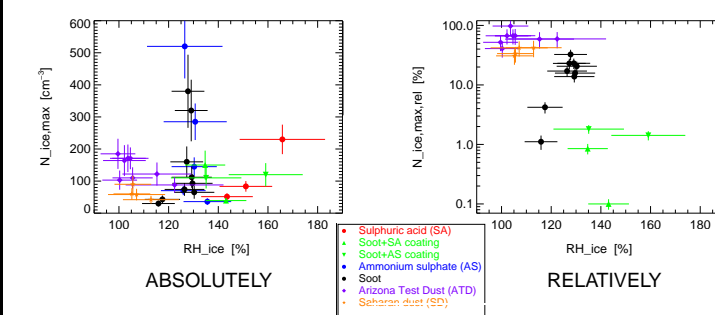
For sulphuric acid aerosol (SA) as well as for the coated soot aerosol (SOOT+SA, SOOT+AS) no results are shown because there are too few experiments at different cooling rates. $(dT/dt)_{\text{inc}}$ refers to the time of the first detection of ice crystals. Note that during AIDA experiments the pumping rate – and not the cooling rate – is controlled. During the pumping period, a heat flux from the warmer walls to the cooler gas phase exists, which decreases the cooling rate with time of pumping. Therefore, $(dT/dt)_{\text{inc}}$ may be different for each experiment. The error bars reflect the uncertainties of the particle measurements. The dependency of the ice crystal number on the cooling rate is for all aerosol types not very clear. As N_{aero} is different for each experiment, there are two parameters possibly influencing $N_{\text{ice,max}}$ and $N_{\text{ice,max,rel}}$. The increase of $N_{\text{ice,max}}$ with stronger cooling rates is most clear for SOOT and SD aerosol. For ATD aerosol there is limited evidence that the total initial aerosol concentration has an influence on the number of ice crystals formed.

Freezing relative humidities over ice $\text{RH}_{\text{ice,nuc}}$



The figure shows $\text{RH}_{\text{ice,nuc}}$ for all aerosol types investigated during AIDA ice nucleation experiments. The error bars reflect the uncertainties of temperature (± 0.3 K) and water vapour measurements ($\pm 5 - 10\%$) and of the exact determination of the onset of freezing ($\pm 5 - 30$ s). In the case of ammonium sulphate aerosol we cannot completely exclude the existence of an externally mixed aerosol containing small amounts of crystalline $(\text{NH}_4)_2\text{SO}_4$ and the lower values of $\text{RH}_{\text{ice,nuc}}$ may be explained by heterogeneous effects (for a detailed discussion see Mangold et al., 2004).

Freezing efficiencies – aerosol types, $\text{RH}_{\text{ice,nuc}}$ and $N_{\text{ice,max}}$ and $N_{\text{ice,max,rel}}$



$N_{\text{ice,max}}$ (left figure) and $N_{\text{ice,max,rel}}$ (right figure) are shown as function of $\text{RH}_{\text{ice,nuc}}$ for the aerosol types investigated during AIDA ice nucleation experiments. $(dT/dt)_{\text{inc}}$ was between -1.3 and -2.0 K min^{-1} and the temperature range was 230–195 K. In the case of $N_{\text{ice,max,rel}}$, the homogeneous freezing experiments are not shown because the respective results for $N_{\text{ice,max}}$ turned out to be independent of N_{aero} . Therefore the respective values of $N_{\text{ice,max,rel}}$ could be shifted by changing N_{aero} . Regarding the results for sulphuric acid aerosol (SA) in the left figure, the increase with increasing $\text{RH}_{\text{ice,nuc}}$ reflects the temperature dependency of $\text{RH}_{\text{ice,nuc}}$ and $N_{\text{ice,max}}$ of the homogeneous freezing process.

SUMMARY

Freezing onset relative humidity

$\text{RH}_{\text{ice,nuc}}$ is lowest ($\approx 110\%$) for ATD and SD aerosol and increases over SOOT ($\approx 120\%$), AS ($\approx 125\%$), and SOOT+SA, SOOT+AS ($\approx 140\%$) to SA aerosol ($\approx 150\%$). The results for SA aerosol confirm the previous findings of Koop et al. (2000) and Möhler et al. (2003). For AS aerosol there remain uncertainties with regard to the exact phase. Coating of dry ice nuclei increases $\text{RH}_{\text{ice,nuc}}$.

Number of ice crystals

Homogeneous freezing: $N_{\text{ice,max}}$ (cm^{-3}) increases with decreasing temperature and stronger cooling rate. This confirms the results of Koop et al. (2000) and Kärcher and Lohmann (2002). Additionally we found no distinct influence of the total initial aerosol concentration N_{aero} on $N_{\text{ice,max}}$.

Heterogeneous freezing: No distinct influence of temperature and cooling rate on $N_{\text{ice,max}}$ and $N_{\text{ice,max,rel}}$ is found. Coating of dry ice nuclei decreases their ice nucleation efficiency. For ATD aerosol there is limited evidence that N_{aero} has an influence on the number of ice crystals formed.

Atmospheric implications

Increasing the fraction of highly efficient ice nuclei of the upper tropospheric total aerosol loading could lead to the formation of cirrus clouds already at higher temperatures, a changed frequency of cirrus occurrence and a changed ice crystal number and size distribution. This affects the radiative properties of the cirrus clouds.